Demosaicked Image Postprocessing Using Local Color Ratios

Rastislav Lukac, *Member, IEEE*, Karl Martin, *Member, IEEE*, and Konstantinos N. Plataniotis, *Senior Member, IEEE*

***Abstract*—A postprocessing method for the correction of visual demosaicking artifacts is introduced. The restored, full-color images previously obtained by cost-effective color filter array interpolators are processed to improve their visual quality. Based on a localized color ratio model and the original underlying Bayer pattern structure, the proposed solution impressively removes false colors while maintaining image sharpness. At the same time, it yields excellent improvements in terms of objective image quality measures.**

***Index Terms*—Bayer pattern, color artifact removing, color filter array (CFA) interpolation, demosaicked image postprocessing, human visual system, subjective evaluation.**

I. Introduction

RECENT times have seen the proliferation of electronic devices such as mobile telephones and personal digital assistants (PDAs) with embedded image capturing capabilities. The majority of these devices use a single charged couple device (CCD) or complementary metal–oxide–semiconductor (CMOS) sensor with a color filter array (CFA). Using the Bayer CFA pattern [1], the sensor produces a two-dimensional array with each spatial location containing only a red (R), green (G), or blue (B) component. Given that each pixel contains one color, spectral interpolation is performed to obtain a full RGB color image. The process of interpolating missing spectral components is known as demosaicking since the restored color image output is obtained using the spatially adjacent CFA data from the input mosaic of the color components [2]–[4].

Due to constraints on cost-effective solutions, the demosaicked images are lacking in sharpness and contain false colors [2], [3], [5]. To complete the task (Fig. 1) and provide the end-user with visually pleasing color output, a demosaicked image postprocessing framework is introduced. In the proposed method, the original uncorrupted Bayer CFA data present in the demosaicked image are exploited along with a localized color ratio model to correct erroneous color components produced by CFA interpolation. The result is an imaging solution capable of producing excellent performance even in image areas with high-frequency characteristics. Simulation analysis and comparative evaluations are provided to illustrate the improvement over published algorithms both in terms of complexity and perceptual image quality.

Manuscript received October 31, 2003; revised December 29, 2003. The work of R. Lukac was supported by a NATO/NSERC Science award. This paper was recommended by Associate Editor H. Gharavi.

The authors are with The Edward S. Rogers Sr. Department of Electrical and Computer Engineering, University of Toronto, Toronto, ON M5S 3G4, Canada (e-mail: lukacr@ieee.org).

Digital Object Identifier 10.1109/TCSVT.2004.828316

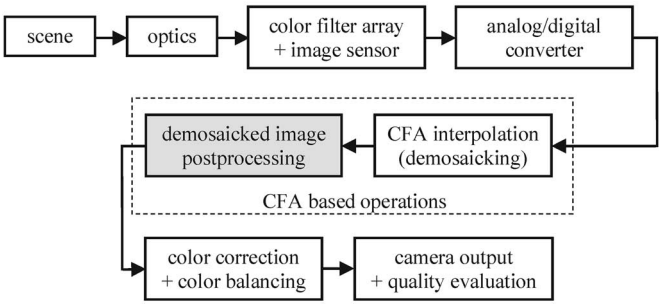

Fig. 1. Simplified digital camera pipeline.

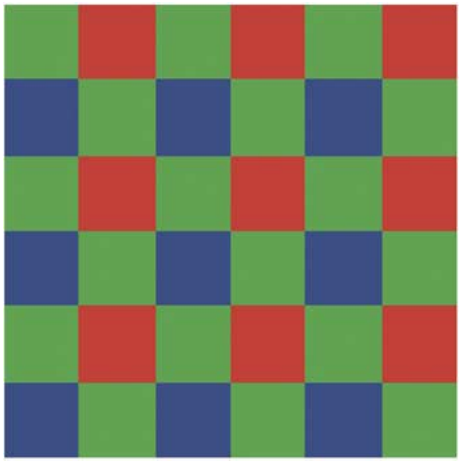

Fig. 2. Bayer CFA Pattern.

II. Demosaicked Color Image Postprocessing

Let us consider a $K_1 \times K_2$ full-color image $\mathbf{x}$: $Z^2 \rightarrow Z^3$ representing a two-dimensional matrix of three-component RGB color samples $\mathbf{x}_{(p,q)} = (x_{(p,q)1}, x_{(p,q)2}, x_{(p,q)3}) \in Z^2$, with $x_{(p,q)1}$ denoting the R component, $x_{(p,q)2}$ denoting the G component, and $x_{(p,q)3}$ indicating the B component. The coordinates $p = 1, 2, \ldots, K_1$ and $q = 1, 2, \ldots, K_2$ denote the spatial position of a pixel in vertical (image rows) and horizontal (image columns) directions, respectively. Assuming the Bayer CFA pattern with the commonly used phase GRGR in the first row (Fig. 2), the demosaicked color image $\mathbf{x}$ has been restored using the R CFA components $x_{(p,q)1}$ located at (odd p, even q), the G CFA components $x_{(p,q)2}$ located at (odd p, odd q) and (even p, even q), and the B CFA components $x_{(p,q)3}$ located at (even p, odd q). Thus, each full-color pixel $\mathbf{x}_{(p,q)}$ consists of an original CFA component and two interpolated components. These estimated components are to be corrected so as to remove

any distortion that may have been introduced during the CFA interpolation procedure.

It should be noted at this point that the proposed methodology can be used with any available phased Bayer CFA and for that matter with any proprietary CFA. Since the CFA structure is readily available to the postprocessing tool designer, the inputs to the postprocessor can be appropriately modified. For the remainder of the paper, the GRGR-phased Bayer array is used as the input to the demosaicked schemes due to its simplicity and common acceptance. Since the original CFA data remain unchanged in the demosaicked images, they can be considered as the input to the postprocessor as well.

It is well known that the sample density of the G component in many RGB color filter array (such as the Bayer pattern) is double that of the R and B components. This is mainly due to the fact that G components are considered to be better representations of the underlying luminance characteristics. It is therefore reasonable to start the postprocessing with the G components.

The postprocessing procedure first updates the estimated G components $x_{(p,q)2}$ at the spatial locations corresponding to the original R or B components as follows:

$$x_{(p,q)2} = x_{(p,q)k} \underset{(i,j)\in\zeta}{\text{mean}} \left\{ \frac{x_{(i,j)2}}{x_{(i,j)k}} \right\} \tag{1}$$

where $\zeta = \{(p-1,q),(p,q-1),(p,q+1),(p+1,q)\}$ and $k=1$ for an original R position (odd p, even q) or $k=3$ for an original B position (even p, odd q). The original G components $x_{(i,j)2}$ are used in conjunction with the interpolated color components $x_{(i,j)k}$ to generate a local color ratio (LCR) description G/R (for $k=1$) or G/B (for $k=3$). In low-quality demosaicked images, unnatural transitions in hue result in many false colors. The variations in hue are often more pronounced than expected in a natural scene due to the fact that neighboring pixels are used in the recovery of unknown values. Due to the trichromatic color representation model and the linear response of digital light sensors, it can be claimed that pixels with similar hues but different intensities should exhibit similar (if not identical) R/G and B/G color ratios [5]–[7]. The proposed LCR creates a model of the hue for the region under consideration and uses it to estimate the G component $x_{(p,q)2}$ based on the original component $x_{(p,q)k}$. It should be noted that the proposed solution avoids extreme transitions in hue in the postprocessed images.

The next step involves the correction of the CFA-interpolated inputs $x_{(p,q)k}$, for R $(k=1)$ located at the original B positions, and B $(k=3)$ located at the original R positions. The corrected G component $x_{(p,q)2}$ of (1) is used to estimate the component $x_{(p,q)k}$ by utilizing the R/G or B/G LCRs as follows:

$$x_{(p,q)k} = x_{(p,q)2} \underset{(i,j)\in\zeta}{\text{mean}} \left\{ \frac{x_{(i,j)k}}{x_{(i,j)2}} \right\} \tag{2}$$

where $\zeta = \{(p-1,q-1),(p-1,q+1),(p+1,q-1),(p+1,q+1)\}$. This operation is similar to (1) except that ζ is adjusted to take into account locations of the original R or B CFA data $x_{(i,j)k}$. The $x_{(i,j)2}$ corresponds to the corrected G component from the previous step.

The postprocessing procedure is completed with the correction of the CFA-interpolated R and B inputs $x_{(p,q)k}$ located at spatial positions corresponding to the original G CFA data. Thus, the postprocessing step (2) is repeated, now utilizing the original G component $x_{(p,q)2}$ and $\zeta = \{(p-1,q),(p,q-1),(p,q+1),(p+1,q)\}$. Two of the values $x_{(i,j)k}$ of (2) are original components and the other two are corrected components previously obtained using (2), whereas $x_{(i,j)2}$ denotes the corrected G components of (1).

Assuming that the digital camera pipeline is sensitive to the complete visible spectrum and produces nonzero Bayer CFA samples, (1) and (2) can be used to complete the postprocessing cycle. However, many interpolation algorithms may introduce zero values by the algorithmic steps performed. Therefore, a commonly used operation for fixing of the zero value problem is to modify the color ratios $x_{(i,j)k}/x_{(i,j)2}$ and $x_{(i,j)2}/x_{(i,j)k}$ as $x_{(i,j)k}/(1+x_{(i,j)2})$ and $x_{(i,j)2}/(1+x_{(i,j)k})$, respectively. It will be shown in the experimental part of this letter that the aforementioned operation is not enough for the well-known LCR-based demosaicking schemes such as [4], [6], [8]. Therefore, a new mechanism is introduced here to avoid singularities in the LCR calculations. To this end, (1) and (2) may be modified as follows:

$$x_{(p,q)2} = -\beta + (x_{(p,q)k} + \beta) \underset{(i,j)\in\zeta}{\text{mean}} \left\{ \frac{x_{(i,j)2} + \beta}{x_{(i,j)k} + \beta} \right\} \tag{3}$$

$$x_{(p,q)k} = -\beta + (x_{(p,q)2} + \beta) \underset{(i,j)\in\zeta}{\text{mean}} \left\{ \frac{x_{(i,j)k} + \beta}{x_{(i,j)2} + \beta} \right\} \tag{4}$$

where β is a constant to be examined later.

It will be shown that although the schemes of [4], [8] utilize an expensive adaptive edge-sensing mechanism in addition to an iterative correction procedure used in [8], they produce significantly worse results compared to the proposed, simple solution defined by (3) and (4). Since fine structural elements are not always wide enough to span the neighborhood used in interpolating the color components, the large dynamics of the CFA data inside ζ prevents the correct recovery of the color information at edges and the demosaicking schemes may introduce color artifacts into the restored image. Using a sufficiently large parameter β, the input LCRs $(x_{(i,j)2}+\beta)/(x_{(i,j)k}+\beta)$ or $(x_{(i,j)k}+\beta)/(x_{(i,j)2}+\beta)$, for $(i,j)\in\zeta$, are projected into the similar values which significantly reduce failures of low-pass (averaging) operators. Thus, the accuracy of the postprocessor defined in (3) and (4) depends only on the multiplicative normalization factor $(x_{(p,q)k}+\beta)$ or $(x_{(p,q)2}+\beta)$, respectively, and the subtractive normalization through $-\beta$. Since $x_{(p,q)k}$ of (3) and $x_{(p,q)2}$ of (4) are the color components which contain high-frequency information at the interpolated locations, the postprocessing preserves the structural content of the image including fine details.

Although in the proposed solution the parameter β can be seen as a tool to eliminate singularities, its practical purpose mainly relates to removal of color artifacts and preservation of fine details. With a sufficiently large value of β, the dynamic range of the color ratios used in the postprocessor decreases. Since natural images vary in color, especially in high-frequency areas, any averaging based interpolator operating on color ratios $x_{(i,j)2}/x_{(i,j)k}$ or $x_{(i,j)k}/x_{(i,j)2}$ introduces an error caused by high variation in the dynamic range of the interpolator's input. Operating on modified LCRs $(x_{(i,j)2}+\beta)/(x_{(i,j)k}+\beta)$ or $(x_{(i,j)k}+\beta)/(x_{(i,j)2}+\beta)$ with sufficiently large β decreases the input's dynamic range inside the local neighborhood ζ, thus, regulating the smoothing process. Since it boosts the performance of the imaging solution,

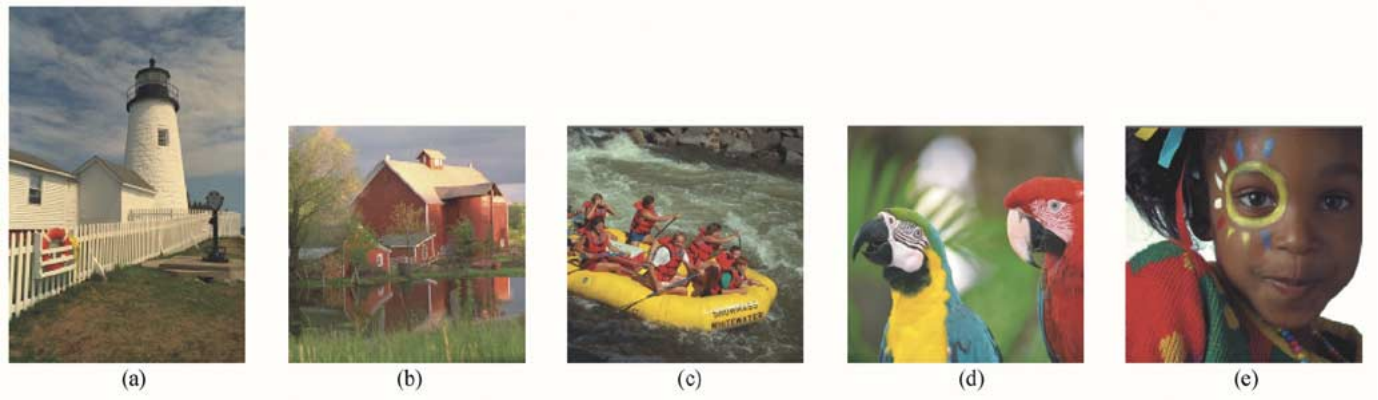

Fig. 3. Test images. (a) *Lighthouse*. (b) *Solitude*. (c) *Rafting*. (d) *Parrots*. (e) *Kid*.

Fig. 4. Zoomed part of the test image *Parrots* corresponding to (a) BI-CFA output ($\mathrm{MAE} = 2.056, \mathrm{MSE} = 29.3, \mathrm{NCD} = 0.0262$), and (b)–(e) the proposed postprocessing method output. (b) $\beta = 0$ ($\mathrm{MAE} = 4.021, \mathrm{MSE} = 576.5, \mathrm{NCD} = 0.0529$), (c) $\beta = 1$ ($\mathrm{MAE} = 1.713, \mathrm{MSE} = 29.1, \mathrm{NCD} = 0.0212$), (d) $\beta = 10$ ($\mathrm{MAE} = 1.483, \mathrm{MSE} = 12.4, \mathrm{NCD} = 0.0195$), and (e) $\beta = 100$ ($\mathrm{MAE} = 1.237, \mathrm{MSE} = 6.6, \mathrm{NCD} = 0.0173$).

the regularization of the dynamic range of the LCRs and its effect on the postprocessing process are examined in this letter. Note that the method can be adapted to other CFAs by simply adjusting the local neighborhood ζ and the concept of the proposed regularization can also be applied to the demosaicking algorithms of [4], [6] and [8], which utilize color ratios.

III. Experimental Results

A number of color images have been used to evaluate the proposed postprocessing framework. As practitioners and image processing researchers are trying to understand the image quality differences between full-color imaging solution and traditional CFA approaches, comparative evaluation of the CFA-sensor based images with full-color images and postprocessed CFA outputs is necessary. The process of comparison adopted in this work follows common practices in the research community and can be summarized as follows.

1) A test set of color images captured using three-sensor devices is built (Fig. 3). Note that most images are 512×512 in size, except the *Lighthouse* image (768×512), and that an 8-bit per channel representation has been used. The image set depicted in Fig. 3 includes images with high-frequency areas where traditionally most demosaicking algorithms fail to provide good results. For example, it is well documented in the literature that the surfaces in the *Lighthouse* image lead to observation of color variations due to aliasing [2].
2) Mosaic versions of the images are created by discarding color information in a GRGR-phased Bayer CFA filter, following standard practices [8]–[10].
3) Demosaicked images are generated using state of the art Bayer CFA interpolation algorithms.
4) Postprocessed demosaicked images are produced using the method described in this letter.[1]
5) Comparative evaluations are performed.

To facilitate the comparisons mentioned in Step 5), the mean absolute error (MAE), the mean square error (MSE) and the normalized color difference criterion (NCD) [11] are used.

In the comparative evaluation considered here, the following CFA-based schemes are employed to obtain the demosaicked images: 1) principle vector method (PVM) [2]; 2) bilinear interpolation (BI) [3]; 3) saturation-based adaptive inverse gradient (SAIG) [4]; 4) constant hue-based interpolation (CHI) [5], [6]; 5) Kimmel's algorithm [8]; 6) color-difference-based effective interpolation (CDEI) [9]; 7) alternating projection (AP) interpolation [10]; 8) median filter interpolation (MFI) [12]; and 9) edge-adaptive color interpolation (ECI) [13]. It should be noted at this point that the above set represents the state of the art in demosaicking procedures and these schemes have been chosen due to their acceptance in peer-reviewed literature.

The evaluation of the factor β introduced in (3) and (4) is shown in Fig. 4. In Fig. 4(b), using $\beta = 0$ exemplifies the effect of the singularities occurring when $x_{(i,j)k} = 0$ in (1) or $x_{(i,j)2} = 0$ in (2). Fig. 4(c)–(e) shows the mitigation of this effect by increasing β of (3) and (4) to 1, 10, and 100, respectively.

Fig. 5 shows the performance of the proposed method depending on β ranging from 1 to 500 with a fixed step size of $\Delta\beta = 1$. Experimentation with a wide set of the images as well as interpolation methods showed that the increase of β eliminates color shifts observed in high-frequency image transitions and results in more true colors. For practical purposes $\beta \geq 128$

[1]The output images visualized in color can be found at the address: www.dsp.utoronto.ca/~lukacr/color1.pdf.

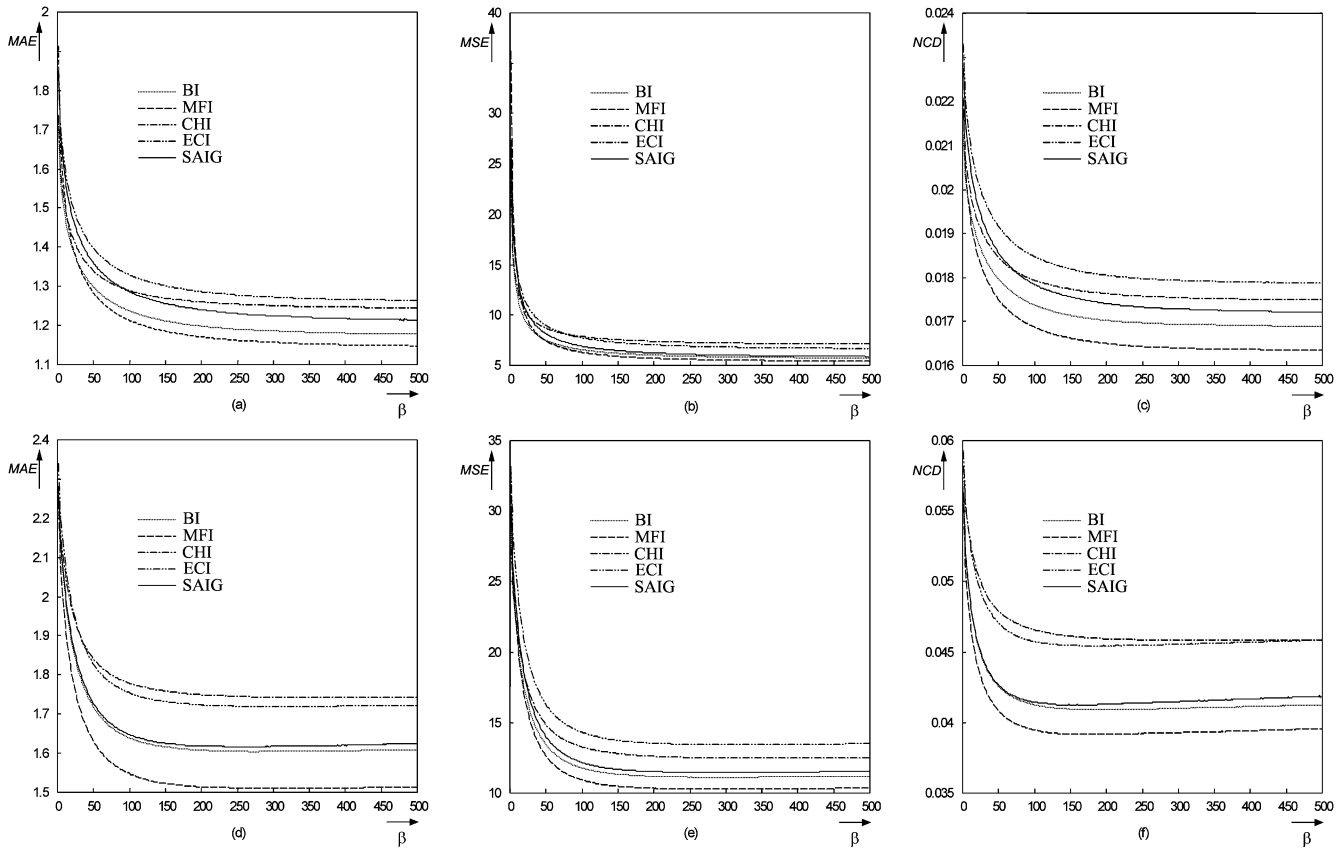

Fig. 5. Performance of the proposed postprocessing method depending on β. (a)–(c) Test image *Parrots*. (d)–(f) Test image *Kid*.

TABLE I
COMPARISON OF THE METHODS USING THE TEST IMAGE *LIGHTHOUSE*

Type	before postprocessing			postprocessed $\beta = 0$			postprocessed $\beta = 128$			postprocessed $\beta = 512$		
Method	MAE	MSE	NCD	MAE	MSE	NCD	MAE	MSE	NCD	MAE	MSE	NCD
BI	4.404	105.8	0.0653	2.416	30.9	0.0390	2.071	19.0	0.0314	2.032	18.0	0.0305
MFI	2.309	31.0	0.0380	2.496	70.1	0.0393	1.777	13.9	0.0271	1.732	12.9	0.0261
CHI	3.437	56.1	0.0501	2.453	35.5	0.0515	2.095	20.4	0.0313	2.068	19.6	0.0307
ECI	2.303	22.6	0.0370	2.058	21.0	0.0342	1.584	9.6	0.0255	1.513	8.5	0.0242
SAIG	2.554	23.9	0.0403	2.426	30.7	0.0410	1.895	11.1	0.0306	1.822	9.8	0.0293
KA	2.227	19.0	0.0365	2.542	34.0	0.0427	1.949	11.8	0.0318	1.857	10.1	0.0303
PVM	2.347	23.1	0.0366	2.614	92.0	0.0415	1.629	9.7	0.0261	1.556	8.7	0.0249
CDEI	2.126	19.3	0.0321	2.419	55.7	0.0387	1.766	13.5	0.0272	1.737	12.6	0.0263
AP	1.456	7.1	0.0237	2.379	64.5	0.0384	1.484	7.7	0.0240	1.415	6.8	0.0228

TABLE II
COMPARISON OF THE METHODS USING THE TEST IMAGE *SOLITUDE*

Type	before postprocessing			postprocessed $\beta = 0$			postprocessed $\beta = 128$			postprocessed $\beta = 512$		
Method	MAE	MSE	NCD	MAE	MSE	NCD	MAE	MSE	NCD	MAE	MSE	NCD
BI	3.843	70.3	0.0579	2.347	27.3	0.0381	2.026	17.6	0.0321	1.996	16.8	0.0320
MFI	2.132	21.8	0.0357	2.370	43.9	0.0384	1.906	15.7	0.0305	1.878	14.8	0.0303
CHI	3.074	41.9	0.0470	2.395	33.7	0.0393	2.105	20.1	0.0335	2.080	19.1	0.0331
ECI	2.477	26.1	0.0387	2.317	26.0	0.0374	1.952	16.0	0.0313	1.899	14.6	0.0308
SAIG	2.701	27.9	0.0418	2.624	33.8	0.0430	2.220	18.0	0.0357	2.175	16.8	0.0350
KA	2.197	24.1	0.0361	2.554	36.4	0.0416	2.092	18.9	0.0335	2.037	17.7	0.0327
PVM	2.696	29.6	0.0419	2.557	60.0	0.0410	1.980	15.7	0.0318	1.947	14.8	0.0314
CDEI	2.038	17.2	0.0329	2.432	44.2	0.0394	1.952	16.6	0.0312	1.916	15.8	0.0308
AP	1.877	13.7	0.0305	2.554	47.5	0.0411	2.014	16.7	0.0323	1.970	15.9	0.0318

(i.e., β larger than half of the dynamic range of the color components) usually produces desirable and robust performance. All subsequent visual results presented in this letter have been obtained using $\beta = 512$ (double the maximum dynamic range of the color components) and this value is also recommended for practical applications.

Tables I–V summarize the objective measurements comparing the original demosaicking results and the postprocessed results, corresponding to the test images shown in Fig. 3. In all cases, the postprocessing operation provides modest to significant improvement. The most significant improvement can be found with the postprocessing of the BI generated images. Before post-

TABLE III
COMPARISON OF THE METHODS USING THE TEST IMAGE *RAFTING*

Type	before postprocessing			postprocessed $\beta = 0$			postprocessed $\beta = 128$			postprocessed $\beta = 512$		
Method	MAE	MSE	NCD	MAE	MSE	NCD	MAE	MSE	NCD	MAE	MSE	NCD
BI	4.730	89.5	0.0753	3.141	79.3	0.0563	2.205	20.0	0.0379	2.187	20.1	0.0387
MFI	2.363	24.0	0.0434	3.339	146.3	0.0571	1.960	18.3	0.0344	1.925	18.3	0.0347
CHI	3.766	58.4	0.0612	3.178	89.8	0.0572	2.254	22.3	0.0387	2.196	20.6	0.0377
ECI	2.939	43.3	0.0492	2.837	57.1	0.0471	2.018	20.1	0.0349	1.945	18.6	0.0350
SAIG	2.975	39.9	0.0643	3.286	102.6	0.0610	2.235	20.9	0.0398	2.144	18.8	0.0387
KA	2.980	53.1	0.0504	3.763	119.2	0.0662	2.559	29.7	0.0454	2.447	27.4	0.0447
PVM	3.066	39.6	0.0504	3.885	216.6	0.0638	2.092	19.5	0.0362	2.039	18.5	0.0357
CDEI	2.241	20.2	0.0396	3.528	163.6	0.0595	2.060	20.9	0.0363	2.016	20.3	0.0362
AP	1.959	19.6	0.0358	3.630	174.8	0.0602	2.085	24.1	0.0368	2.028	23.2	0.0368

TABLE IV
COMPARISON OF THE METHODS USING THE TEST IMAGE *PARROTS*

Type	before postprocessing			postprocessed $\beta = 0$			postprocessed $\beta = 128$			postprocessed $\beta = 512$		
Method	MAE	MSE	NCD	MAE	MSE	NCD	MAE	MSE	NCD	MAE	MSE	NCD
BI	2.056	29.3	0.0262	4.021	576.5	0.0529	1.221	6.3	0.0172	1.163	5.7	0.0169
MFI	1.169	6.8	0.0172	4.042	579.9	0.0529	1.195	6.0	0.0167	1.131	5.3	0.0163
CHI	1.694	16.7	0.0223	4.059	577.5	0.0535	1.277	7.7	0.0178	1.233	7.0	0.0174
ECI	1.566	16.2	0.0207	1.921	34.2	0.0239	1.311	7.4	0.0182	1.250	6.6	0.0178
SAIG	1.714	11.6	0.0224	4.501	584.1	0.0594	1.621	9.0	0.0226	1.582	8.2	0.0223
KA	2.643	91.9	0.0357	4.673	589.8	0.0615	1.961	17.2	0.0269	1.951	17.1	0.0268
PVM	1.489	11.1	0.0199	4.162	583.8	0.0546	1.244	6.3	0.0173	1.999	5.6	0.0169
CDEI	1.176	5.8	0.0170	4.157	583.5	0.0543	1.281	7.1	0.0178	1.231	6.3	0.0180
AP	1.184	5.5	0.0167	4.261	588.0	0.0553	1.342	7.8	0.0184	1.286	7.0	0.0181

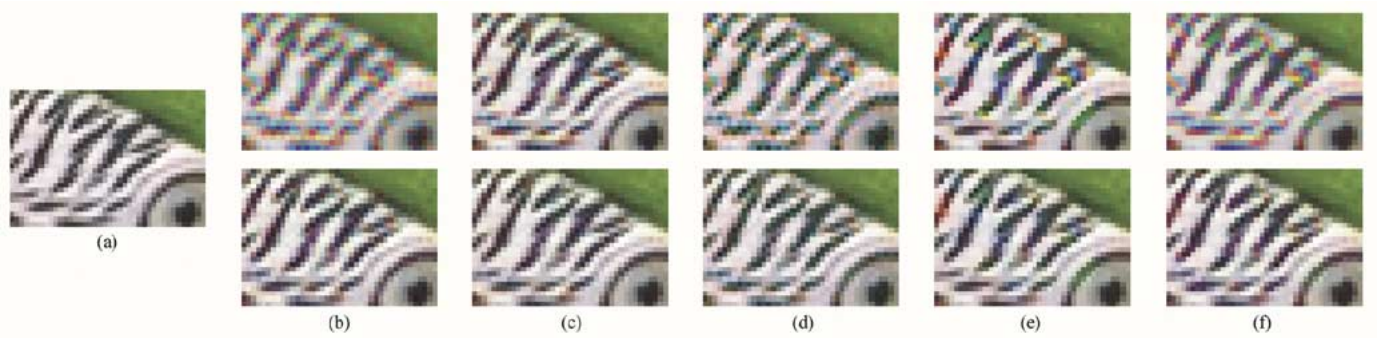

Fig. 6. Enlarged parts of the original *Parrots* image (a), and the restored outputs (b)–(f) before (top line) and after (bottom line) postprocessing: (b) BI, (c) MFI, (d) CHI, (e) ECI, and (f) SAIG.

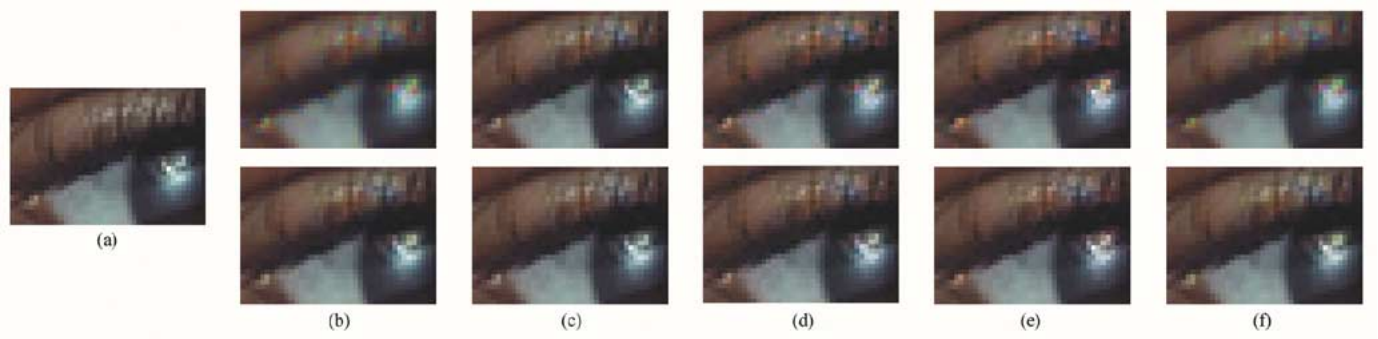

Fig. 7. Enlarged parts of the original *Kid* image (a), and the restored outputs (b)–(f) before (top line) and after (bottom line) postprocessing: (b) BI, (c) MFI, (d) CHI, (e) ECI, and (f) SAIG.

processing, the MFI, PVM, CDEI, and AP generated the highest quality full-color images. In these situations, the postprocessing still provided modest improvement. The smallest improvement is obtained when the method is applied to the restored output corresponding to the AP scheme. Zero or close values introduced into the restored output can be prohibitive to obtain the improvement through (1) and (2), where β is omitted. Note that these operations are equivalent to (3) and (4) with $\beta = 0$. However, if $\beta = 128$ (half dynamic range) is used, significant improvements are achieved via (3) and (4). Additional improvement is obtained using $\beta = 512$ (double dynamic range), which is then used for generating the postprocessed outputs depicted in Figs. 6–9.

Figs. 6–7 show zoomed-in portions of the test images in areas that are typically problematic for CFA-based interpolation schemes. False color distortion is quite evident for BI, CHI, ECI, and SAIG. Upon applying the proposed procedure, the

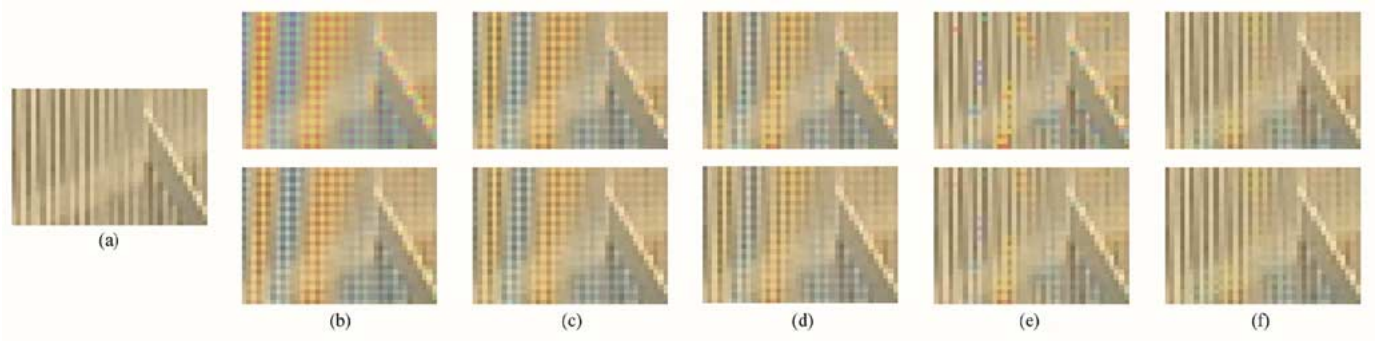

Fig. 8. Enlarged parts of the *Lighthouse* image suffering from aliasing: (a) the original image, (b)–(f) the restored outputs before (top line) and after (bottom line) postprocessing: (b) BI, (c) ECI, (d) KA, (e) PVM, and (f) AP.

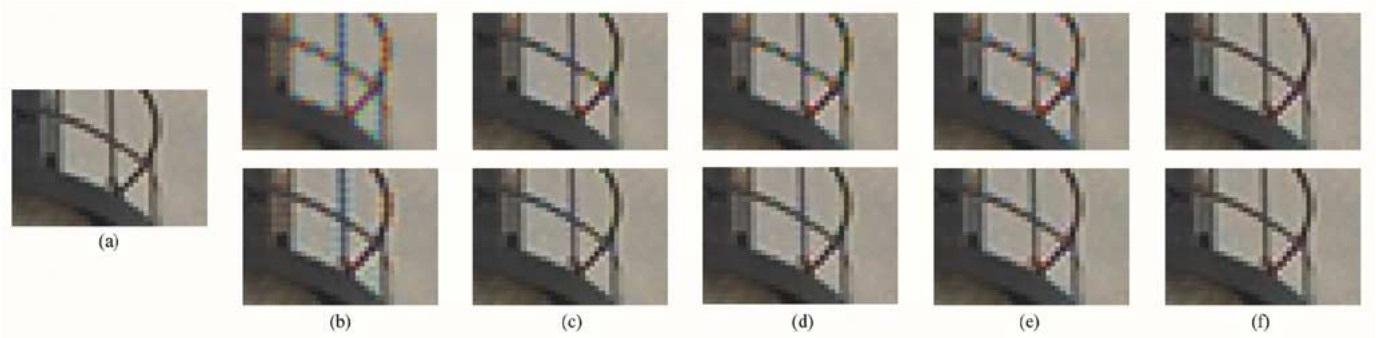

Fig. 9. Enlarged parts of the results corresponding to the *Lighthouse* image: (a) the original image, (b)–(f) the restored outputs before (top line) and after (bottom line) postprocessing: (b) BI, (c) ECI, (d) KA, (e) PVM, and (f) AP.

TABLE V
COMPARISON OF THE METHODS USING THE TEST IMAGE *KID*

Type	before postprocessing			postprocessed $\beta = 0$			postprocessed $\beta = 128$			postprocessed $\beta = 512$		
Method	MAE	MSE	NCD	MAE	MSE	NCD	MAE	MSE	NCD	MAE	MSE	NCD
BI	3.066	42.6	0.0697	2.049	43.6	0.0611	1.623	11.5	0.0410	1.633	11.6	0.0421
MFI	1.715	12.7	0.0451	2.385	49.3	0.0598	1.530	10.6	0.0392	1.514	10.4	0.0395
CHI	2.814	37.3	0.0674	2.857	130.6	0.0753	1.765	13.0	0.0462	1.748	12.7	0.0461
ECI	2.543	34.5	0.0612	2.529	72.3	0.0620	1.738	13.9	0.0455	1.723	13.5	0.0458
SAIG	2.755	34.5	0.0620	3.100	135.0	0.0840	2.108	16.1	0.0607	2.108	15.8	0.0611
KA	2.660	37.3	0.0709	3.390	146.8	0.0916	2.349	20.9	0.0687	2.355	21.0	0.0696
PVM	2.360	25.9	0.0559	2.728	91.0	0.0663	1.687	12.5	0.0425	1.664	12.1	0.0423
CDEI	1.658	11.7	0.0429	2.463	68.9	0.0619	1.530	10.7	0.0398	1.527	10.7	0.0404
AP	1.646	11.9	0.0440	2.665	83.7	0.0648	1.663	13.0	0.0430	1.658	12.9	0.0440

effect is completely removed. In conjunction with the removal of false colors, an increase in image sharpness is observed. For the MFI scheme the false color artifacts are not as evident, but applying the postprocessing operation has no detrimental effect on the image fidelity and a modest increase in sharpness is evident. The most modest results are shown in Fig. 7, where the postprocessing still leaves a moderate amount of false color artifacting. However, the postprocessing provides improvement when compared to the images obtained using the CFA interpolators. In this case, the problematic region is low-contrast, making the artifacts significantly less visually disturbing.

Figs. 8 and 9 allow for the visual comparison of the methods considered here when the test image *Lighthouse* is used. As it can be seen, sophisticated demosaicking algorithms such as KA and PVM produce better results than the simplistic methods BI and ECI. The postprocessor attached to BI or ECI results in excellent improvement in terms of performance. For example, the BI interpolator was unable to remove the aliasing artifacts around the *picket fence* area of the image (Fig. 8). The invocation of the postprocessor resulted in a dramatic improvement in this area. It was noticed during the subjective evaluation tests that the techniques such as KA and PVM have done an excellent job restoring the *picket fence* or the *home siding* portion of the image, but they have introduced impairments and artifacts in other areas. Fig. 9 is used here to illustrate the undesirable side-effect of the demosaicking process. As can be seen, the postprocessor was able to cancel the side-effects and produced an image with no impairments or visual artifacts.

Apart from the numerical behavior (actual performance) of any algorithm, its computational complexity is a realistic measure of its practicality and usefulness. Therefore, the proposed method is analyzed here in terms of elementary operations, namely additions (ADDs), subtractions (SUBs), multiplications (MULTs) and divisions (DIVs). From (3) or (4) it can be seen the postprocessing of any interpolated color component $x_{(p,q)k}$, for $k = 1, 2, 3$, requires only 12 ADDs, 1 SUB, 1 MULT and

5 DIVs. This suggests that the proposed method introduces only a moderate level of computational overhead. Note that using $\beta \leq 256$ increases the hardware requirements on the sample representation during the processing cycle with one more bit per color component $x_{(p,q)k}$, for $k = 1, 2, 3$. If $256 < \beta \leq 768$, ten bits per color component $x_{(p,q)k}$ are necessary. Therefore, the increase in β larger than 768 is not recommended as it increases the cost of postprocessing and does not introduce additional improvements in performance. Note that (3) and (4) normalize the postprocessed output into the range represented with eight bits per color component. The execution of the developed postprocessing tool on a personal computer with an Intel Pentium IV 2.40 GHz CPU, 512 MB RAM, Windows XP operating system and MS Visual C++ 5.0 programming environment, took on average 0.311 sec per 512×512 input image.

Summarizing the findings of the experimental comparisons, we can claim the following.

1) The proposed postprocessing procedure provides modest to significant improvement in image quality in all cases.
2) When it is used with simple interpolation schemes such as BI or MFI, the postprocessor provides significant improvement by removing false color artifacts and increasing sharpness.
3) The postprocessor was able to improve the performance of complicated demosaicking solutions by removing color artifacts still present after demosaicking.
4) The combination of interpolator and postprocessor restores chrominance information of the image; using the design parameter β corresponding to double dynamic range $(\beta = 512)$ of the color components, color moire can be eliminated to a large degree.
5) The postprocessor can be easily implemented either in software or hardware.

IV. Conclusion

A technique for postprocessing CFA-based, interpolated images was introduced. The underlying Bayer structure from the original image is utilized along with a local color ratio model. For all test images, the scheme reduced or completely removed false color artifacts while increasing image sharpness. The computational simplicity of the operation suggests that it can be used in cost-effective single-sensor solutions. Given such an option, the postprocessing operation should directly follow the demosaicking algorithm in the digital camera pipeline. Combined with a demosaicking scheme, the proposed method can be seen as a correction of the CFA interpolation algorithm.

References

[1] B. E. Bayer, "Color imaging array," U.S. Patent 3 971 065, July 20, 1976.
[2] R. Kakarala and Z. Baharav, "Adaptive demosaicing with the principle vector method," *IEEE Trans. Consumer Electron.*, vol. 48, pp. 932–937, Nov. 2002.
[3] P. Longere, X. Zhang, P. B. Delahunt, and D. H. Brainard, "Perceptual assessment of demosaicing algorithm performance," *Proc. IEEE*, vol. 90, pp. 123–132, Jan. 2002.
[4] C. Cai, T. H. Yu, and S. K. Mitra, "Saturation-based adaptive inverse gradient interpolation for Bayer pattern images," in *Proc. IEE—Vision, Image, Signal Process.*, vol. 148, June 2001, pp. 202–208.
[5] R. Ramanath, W. E. Snyder, and G. L. Bilbro, "Demosaicking methods for Bayer color arrays," *J. Electron. Imaging*, vol. 11, pp. 306–315, July 2002.
[6] D. R. Cok, "Signal processing method and apparatus for producing interpolated chrominance values in a sampled color image signal," U.S. Patent 4 642 678, Feb. 10, 1987.
[7] M. Chapron, "A new chromatic edge detector used for color image segmentation," in *Proc. IEEE Int. Conf. Pattern Recognition*, vol. 3, Sept. 1992, pp. 311–314.
[8] R. Kimmel, "Demosaicing: Image reconstruction from color CCD samples," *IEEE Trans. Image Processing*, vol. 8, pp. 1221–1228, Sept. 1999.
[9] S. C. Pei and I. K. Tam, "Effective color interpolation in CCD color filter arrays using signal correlation," *IEEE Trans. Circuits Syst. Video Technol.*, vol. 13, pp. 503–513, June 2003.
[10] B. Gunturk, Y. Altunbasak, and R. Mersereau, "Color plane interpolation using alternating projections," *IEEE Trans. Image Processing*, vol. 11, pp. 997–1013, Sept. 2002.
[11] K. N. Plataniotis and A. N. Venetsanopoulos, *Color Image Processing and Applications*. Berlin, Germany: Springer–Verlag, 2000.
[12] W. T. Freeman, "Median Filter for Reconstructing Missing Color Samples," U.S. Patent 4 724 395, Feb. 9, 1988.
[13] B. S. Hur and M. G. Kang, "High definition color interpolation scheme for progressive scan CCD image sensor," *IEEE Trans. Consumer Electron.*, vol. 47, pp. 179–186, Feb. 2001.